Optical Trapping, Optical Binding, and Rotational Dynamics of Silicon Nanowires in Counter-Propagating Beams

Maria G. Donato,[*,†,§] Oto Brzobohatý,[‡,§] Stephen H. Simpson,[‡,§] Alessia Irrera,[†] Antonio A. Leonardi,[†,¶] Maria J. Lo Faro,[†] Vojtěch Svak,[‡] Onofrio M. Maragò,[*,†] and Pavel Zemánek[*,‡]

†*CNR-IPCF, Istituto per i Processi Chimico-Fisici, I-98158, Messina, Italy*

‡*Institute of Scientific Instruments of the CAS, Kralovopolska 147, 61264 Brno, Czech Republic*

¶*Dipartimento di Fisica e Astronomia, Università di Catania, I-95123, Catania, Italy*

§*These authors contributed equally to the work.*

E-mail: maria.donato@cnr.it; onofrio.marago@cnr.it; zemanek@isibrno.cz

Abstract

Silicon nanowires are held and manipulated in controlled optical traps based on counter-propagating beams focused by low numerical aperture lenses. The double-beam configuration compensates light scattering forces enabling an in-depth investigation of the rich dynamics of trapped nanowires that are prone to both optical and hydrodynamic interactions. Several polarization configurations are used, allowing the observation of optical binding with different stable structure as well as the transfer of spin and/or orbital momentum of light to the trapped silicon nanowires. Accurate modeling based on Brownian dynamics simulations with appropriate optical and

hydrodynamic coupling confirms that this rich scenario is crucially dependent on the non-spherical shape of the nanowires. Such increased level of optical control of multi-particle structure and dynamics open perspectives for nanofluidics and multicomponent light-driven nanomachines.

Keywords

Optical trapping, optical binding, silicon nanowires, light-driven rotations, light angular momentum

The precise and reliable manipulation of single or multiple nanostructures has important consequences for contemporary nanoscience.[1] In this regard, optical forces[2–4] exerted by light beams can play a key role.[5–8] Light can be used to trap,[2–4] push[9–11] or bind[12–15] a great variety of dielectric,[16–23] semiconducting,[24–31] carbon-based,[32–35] plasmonic,[36–42] metal-dielectric hybrid,[43,44] and biological[45–47] nano- and micro-particles, directly in liquid, air or vacuum environment.

In single-beam optical trapping, *i.e.*, standard optical tweezers,[3,4] a laser beam is generally focused by a high numerical aperture (NA) objective to a diffraction-limited spot. Thus, a nanoparticle can be trapped near the focal point by optical forces associated with the high intensity gradients surrounding the focal region. These gradient forces generally overcome the unavoidable light scattering forces which tend to push the particle in the (axial) propagation direction, downstream of the beam focus.[8] However, for small nanoparticles this destabilizing effect of scattering forces combined with thermal fluctuations can be large enough to overwhelm trapping forces for reasonable incident laser powers.[6] Morphology,[42] material composition,[48] and enhanced optical properties of nanoparticles can increase optical trapping at the nanoscale – for example optical forces can be enhanced by the particle opto-plasmonic response,[36–42] or by highly anisotropic geometries, such as in nanowires,[25–28,49] carbon nanotubes,[32,33] graphene,[34] and layered materials.[11] Alternatively, the detrimental effects of scattering forces can be suppressed through the use of two counter-propagating

beams.[2] These dual-beam traps are based on the use of low NA lenses and allow trapping of nanoparticles with reduced incident power in a focal region that is wider than for standard optical tweezers.[5,14,42] When the beams are linearly polarized in the same direction, a standing wave trap[50] is formed and many equilibrium positions are generated by the interference fringes that form along the beam axis.[51] Optical trapping with counter-propagating beams can also be obtained with less alignment effort if a low NA objective and a mirror are used,[52,53] by using two single-mode or photonic crystal fibers without any beam focusing[54–56] or employing hollow-core photonic fibers filled with liquid or air.[57,58]

The dual-beam geometry is particularly suitable for the investigation of optically mediated self-arrangement of multiple particles along the beam axis, the so-called longitudinal optical binding effect.[13,18,59] While optical binding of spherical particles has been extensively studied, both theoretically[13,15,60–68] and experimentally[15,18,19,56,59,69–80] in lateral or longitudinal geometries, optical binding of non-spherical, chiral, or birefringent particles is still in its infancy both experimentally[6,21,81,82] and theoretically.[31,61,83,84] Moreover, optical binding between more complex, lower symmetry objects, offers perspectives to the optically controlled generation of complex functional microstructures, *e.g.*, to deliver particles,[79] form optically bound rotors[21,74] or tunable two-dimensional lattices of optically bound microstructures.[75]

In this work, we use counter-propagating Gaussian and Laguerre-Gaussian beams with three different types of polarizations: parallel linear polarization (PLP), crossed linear polarization (XLP), and opposite circular polarization (CP). We observe a rich spectrum of localization, orientation, and rotation possibilities for individual and optically bound silicon nanowires (SiNWs). We investigate experimentally the stability configurations and nanowire dynamics in the trap. Thus, we contrast our observations with accurate theoretical simulations based on Brownian dynamics of the optical and hydrodynamic interactions performed with parameters close to the experimental ones.

SiNWs are synthesized by metal assisted chemical etching[85,86] (MACE) (see section S4.1 in the Supp. Info. for more details) using a solution of silver nitrate ($AgNO_3$) and hydrogen

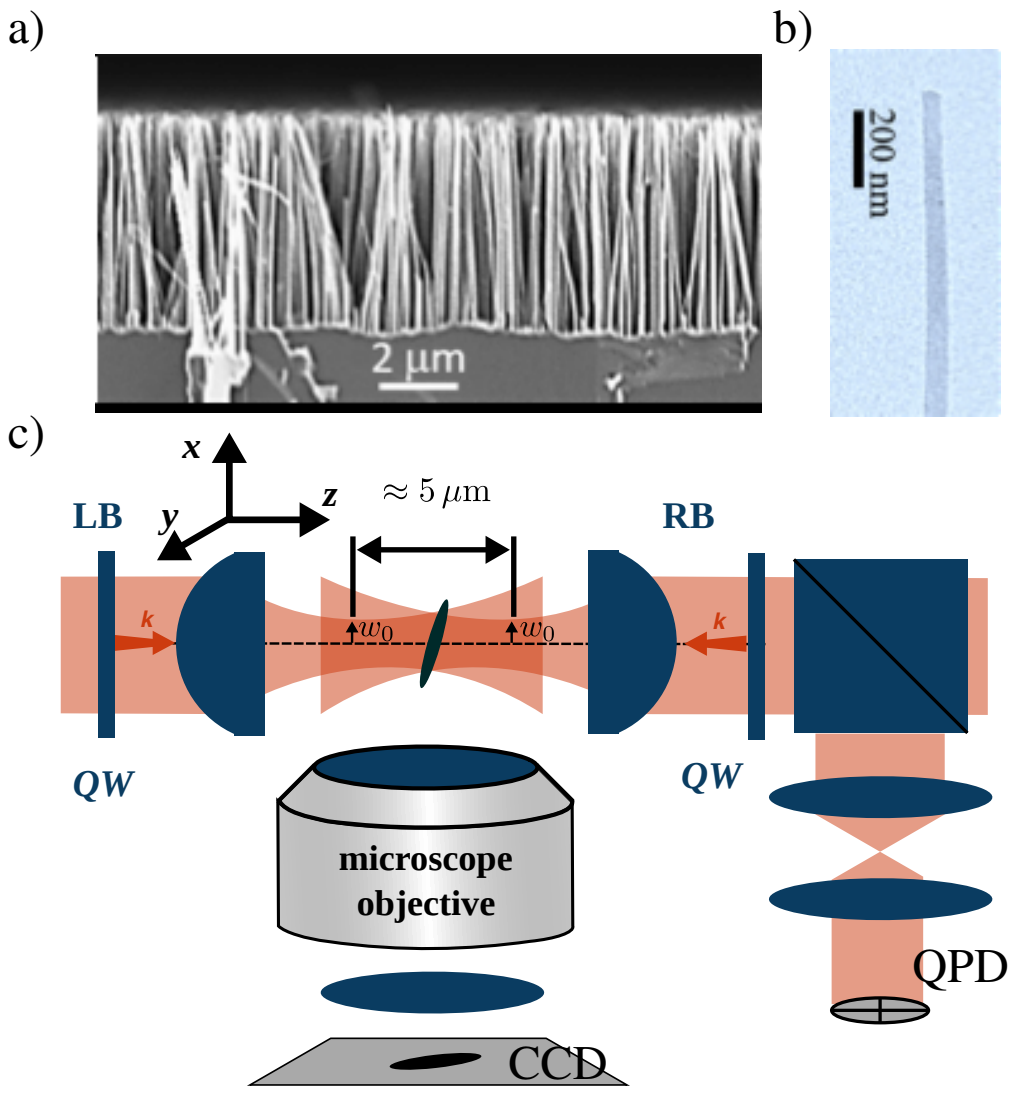

Figure 1: (a) Cross section SEM image of SiNWs obtained after the wet etching of the silicon substrate. The image displays a dense and uniform distribution of NWs, having approximately 6 μm length. (b) TEM microscopy image of the top region of a SiNW, showing a good uniformity and a diameter of $D = 78 \pm 16$ nm as obtained from TEM analysis. (c) Sketch of the dual-beam optical trap. This is composed of two counter-propagating laser beams (left-hand beam, LB, and right-hand beam, RB) focused by two aspheric lenses (NA=0.5, w_0 beam waist). Beam polarizations can be set on each beam by quarter wave plates (QWs). The two beam foci are slightly displaced (approximately 5 μm) along the beam propagation direction to increase axial trapping stability. Optically trapped SiNWs are observed using a microscope, composed by a long working distance objective, tube lens (focal length 200 mm), and CCD camera. 10% of the left-hand beam (LB) intensity is reflected by a (10:90) non-polarizing beamsplitter. In order to track SiNWs positions, the back-focal plane of the right aspheric lens is imaged on a quadrant photodiode (QPD) using a telescope.

fluoride (HF). A bulk silicon substrate n-doped (1.5 Ω cm) and (100)-oriented is immersed in an aqueous solution containing 0.02 M of $AgNO_3$ as metal precursor and 5 M of HF as etching agent. Here the silver salts dissociate, thus realizing a precipitation of silver nanoparticles that randomly distribute on the silicon surface. Locally, just underneath the region covered by metal nanoparticles, silicon oxide is formed that is subsequently removed by HF. As a consequence, silver nanoparticles sink into the silicon bulk, leading to the formation of SiNWs. The presence of silver contamination is effectively removed from SiNWs with a proper chemical etching that can either use nitric acid[87,88] or ammonium hydroxide.[86] To fully remove silver residues from our SiNWs, we soaked the sample for 10 minutes in nitric acid (90%) and cross-verified the absence of silver onto the SiNWs by both Rutherford backscattering spectrometry (RBS) and Energy Dispersive X-ray spectroscopy (EDX) analyses (see section 4 in the Supp. Info.). RBS is performed by using a source of He^+ ion accelerated with an HVEE singletron at the energy of 2 MeV and deflected onto a home-made scattering chamber where the backscattered ions were collected and analyzed by a multichannel analyzer for the spectra acquisition. EDX is carried out onto HNO_3 etched SiNWs by means of a ZEISS scanning electron microscope equipped with an Oxford module for EDX. Cross sectional images of the SiNWs array are obtained by using a field emission scanning electron microscope (SEM) Zeiss Supra 25 (Fig. 1a), showing that SiNWs formed are approximately 6 μm long. The diameter of the samples is obtained from transmission electron microscopy (TEM) analysis that is realized by a FEI Tecnai 12 electron microscope obtaining a diameter distribution (see Supporting Information) that yields an average value of $D = 78$ nm with a standard deviation of 16 nm.

The experimental setup[74] we use for optical trapping is sketched in Fig. 1c. We use an infrared laser source (IPG, YLM-10-1064-LP-SP) with a vacuum wavelength of 1064 nm. Two horizontally counter-propagating laser beams are generated by a holographic mask imprinted onto a single spatial light modulator (SLM) and transferred by relay optics. The SLM enables us to alter the waists of the two beams independently in a range 1.8-3.8 μm

(Rayleigh range within 8-45 μm) and control the total power at the sample during the experiments in a range of 25-80 mW. This corresponds to an irradiance of about 0.1-1.6 MW/cm^2, with the largest irradiance corresponding to the smallest waist size (1.8 μm). The two beam foci are slightly displaced (approximately 5 μm) along the beam propagation direction to increase axial trapping stability. Their respective polarization states are controlled with half and quarter waveplates. The propagation direction is parallel to the z-axis, linearly polarized waves are polarized in the x (vertical polarization) or y (horizontal polarization) direction, while for circularly polarized beams, the electric field vector rotates in the x-y plane. Where circularly polarized beams are used, the counterpropagating beams have opposite handedness so that the electric field vectors rotate in the same sense. Optical trapping experiments are conducted in water. The first step is to scratch the SiNWs from the substrate. This breakage can cause occasional shortening of the SiNWs' length. As described below, the resulting variation in the length of the nanowires allowed us to observe a greater range of behaviour in our optical traps. Thus, the scratched SiNWs are dispersed in deionized water with the aid of sodium dodecyl sulfate (SDS) surfactant inside a glass squared capillary (Vitrocell) with an inner size of 50 μm. The capillary is inserted into the optical field of focused, counter-propagating laser beams. The imaging and dynamics of the trapped SiNWs are observed by a CCD camera (Basler Ac640-750) from a direction (y) perpendicular to the propagation z-axis. Additionally a quadrant photodiode (Thorlabs PDQ80A) is aligned to collect the back focal plane interferometry and tracking signals from the trapping region enabling a complementary analysis[89] of Brownian motion, optical forces, and rotational dynamics of the trapped samples. Despite the fact that absorption of water at our trapping wavelength might induce thermal fluid flow, this phenomenon is highly suppressed by the use of the thin capillary.[74] Native silicon is also a low absorber in the near infrared, but at our irradiance some small temperature effects might be expected.[90,91] However, the counterpropagating configuration and a waist wider than typical single-beam optical tweezers ensure temperature effects smaller than a couple of degrees,[91] as well as isotropic heating

with consequent limited influence of thermophoretic flow along the SiNWs' axial direction.

Accurate calculations and modelling are performed under isothermal conditions using the approach described in Simpson *et al.*,[31] and in the Supporting Information, which also includes a comprehensive stability analysis for single nanowires in counter-propagating beams as well as analysis of optical binding effects. In particular, the behaviour of the particles in the counter-propagating beam traps is determined by the interplay of coupled, optical and hydrodynamic forces acting on the nanowires. To capture these effects in the model, each nanowire is represented by an array of small beads, or cells, which act as the loci for both hydrodynamic and optical disturbances. The beads from different nanowires are coupled through interaction tensors, the dipole interaction tensor[92] for the optical regime, and the Rotne-Prager tensor for hydrodynamics. Solution of the resulting many-body problem allows us to evaluate the influence of each bead and, subsequently, the optical force and viscous drag with which they are each associated. By summing these effects in an appropriate way, we compute the optical forces and torques on each nanowire as well as the translational and rotational viscous drag. In this way, the model nanowires act as continuous, rigid bodies with realistic, fully coupled, optical and hydrodynamic interactions. As the lattice of beads used to represent the nanowires is refined, the calculation converges on continuum results. Finally, evaluating the hydrodynamic and optical forces allows us to integrate the Langevin equation for the system, including thermal fluctuations.

Parallel and crossed linear polarization. In the absence of gradient forces, nanowires tend to align with the electric polarization.[93] Instead, in a tightly focused single beam trap, SiNWs tend to align with the beam axis,[26,94,95] unless they are so short that they do not protrude beyond the diffraction limited beam size,[94] that for a wavelength of 1064 nm corresponds to SiNWs shorter than about $\sim 0.4\mu$m. However, in our counter-propagating beam traps, the beam waist is relatively wide (1.8-3.8 μm) and the nanowires can adopt a variety of orientations because of the interplay between these polarization and gradient intensity aligning torques.

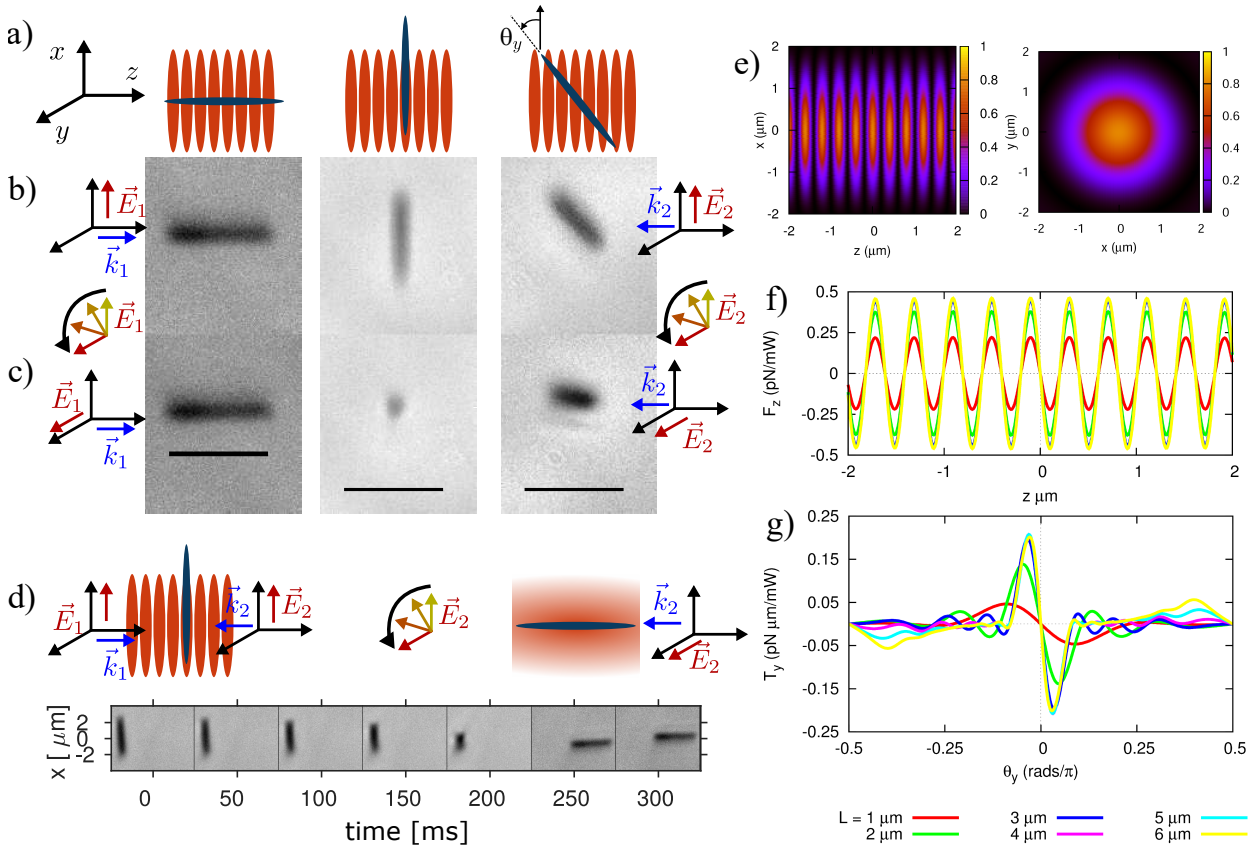

Figure 2: Optical trapping and manipulation of SiNWs in parallel (PLP) and crossed (XLP) linear polarization of counter-propagating beams. In (a) we sketch the different orientations of a trapped SiNW in PLP configuration and as observed in (b): parallel (left), perpendicular (middle), or tilted (right) with respect to the beams propagation axis. In (c) the polarization of both beams is rotated from vertical to horizontal (see Movie 1). As a consequence the alignment of a trapped SiNW is unchanged for parallel orientation (left), while is rotated for the case of perpendicular or tilted orientation with respect to the beam axis due to the polarization optical torque controlling these orientation. Scale bars correspond to 5 μm. In (d), when the configuration is switched from PLP to XLP, the orientation of the SiNW with respect to the beam propagation axis is switched from perpendicular to parallel. The trap parameters are set to a beam waist of $w_0 = 1.8\,\mu$m, and a total power at the sample of about 80 mW. (e) Calculated field intensity for PLP configuration showing the standing wave interference pattern along the propagation direction (left) and the transverse Gaussian intensity profile (right). (f) Calculations of the axial optical force, F_z, for SiNWs trapped and oriented along the polarization axis x, showing that trapping points correspond to the standing wave intensity maxima. (g) Calculations of optical torque component, T_y, for varying θ_y, the angle that the nanowire makes with the polarization direction (x-axis). Equilibrium orientations occur when $T_y = 0$ and $dT_y/d\theta_y < 0$. There are two obvious orientational equilibria. The first, $\theta_y = 0$, in which the SiNW aligns with the polarization direction, has a narrow angular range (about ± 12 degrees). The second, $\theta_y = \pi/2$, in which the nanowires align with the beam axis, is available to longer SiNWs and has a much wider angular range (about ± 45 degrees for 6 μm SiNWs). The graph also shows a number of oblique equilibria, dependent on the length of the wire.

In the case of counter-propagating beams having parallel linear polarization (PLP), a standing wave is formed with a series of high intensity fringes distributed along the beam z-axis (see fig. 2 and Supporting Information S3.1) and parallel to the x-y plane. In this geometry a competition between the polarization torque, transverse high intensity gradients, and elongated high intensity structure of the counter-propagating beams occurs. In fact, as shown in Fig. 2a-c, we observe a range of stable orientations for individual SiNWs in the trap. For SiNWs with a length of several microns, the most stable orientation is observed when they align with the beam z-axis, *i.e.*, along the averaged high intensity profile of the counter-propagating beams. This behaviour is reproduced theoretically in Figure 2 (g) and in the Supporting Information S3.1 and S3.3. As nanowires are rotated about axes perpendicular to the beam axis (*i.e.*, axes in the xy plane), they intercept varying numbers of bright intensity fringes, generating series of tilted equilibrium configurations. The equilibrium when the axis is parallel to the polarization ($\theta_y = 0$) is the strongest, but it has a low angular range (± 12 degrees), *i.e.*, if the wire orients outside this range, the equilibrium is lost. The equilibrium when the wire is parallel to the z axis ($\theta_y = \pi/2$) is weaker in that the restoring torques are weaker, but it has a much wider angular range (about 50 degrees for the 6 μm nanowire). For this reason, the equilibrium with the SiNW axis parallel to the beam axis is the one that is most commonly observed. There are a series of oblique equilibrium orientations, that depend on the length of the nanowire. For very short nanowires, the only equilibrium occurs when the SiNW aligns with the polarization. Stable orientations can also occur when long SiNWs align parallel to the polarization x-direction or at an angle close to 45 deg in the x-z plane (Figs. 2a-b). We confirm this strong influence of the polarization torque by rotating the beams polarization axis from x to y and observing the consequent controlled tilt of the trapped SiNW (Figs. 2c) in radially symmetric Gaussian beam and even in Gaussian beams with significant elliptical transverse beam profile (with beam waists $w_{0,x} = 0.9\,\mu$m and $w_{0,y} = 8\,\mu$m). Stiffness coefficients for the SiNWs can be estimated from the optical force density, under the Rayleigh-Gans approximation (see

Supporting Information S3.1.2): the extreme aspect ratio of the wires means that the forces on the wire are relatively insensitive to translations parallel to its axis, but vary rapidly with displacements in orthogonal directions.[26,95] Thus the stiffness coefficient in the x direction (parallel to the wire and to the polarization) decreases exponentially with increasing wire length (for a wire of length L, $k_x \sim L\mathrm{e}^{-L^2/2w_0^2}$), whilst the stiffness in the y direction is about three orders of magnitude greater, and approaches a constant value, with increasing length. For example, a wire of length 6 μm gives $k_x/k_y \approx 1.3 \times 10^{-3}$. Furthermore, the angular stiffness for tilt around the y-axis (*i.e.*, out of the standing wave high intensity fringe) is about two orders of magnitude stronger than that for rotations around z axis (*i.e.*, in the plane of the high intensity fringe). This is confirmed theoretically in Figure S3 of the Supplementary Information, S3.1.1.

However, if the polarization of only one beam is adiabatically rotated, a SiNW originally trapped in the transverse plane and oriented along the polarization axis rotates until the polarizations of the beams are perpendicular (XLP). When this crossed polarization geometry is reached, the SiNW orientation switches fast to a longitudinal orientation along the z-axis (see Fig. 2d). This effect is caused by the disappearance of the intensity fringes, which no longer confine the nanowire in the transverse plane. Under these circumstances the model confirms that intensity gradient torques tend to dominate for long nanowires, so that they align the nanowires along the beam axis (see Supplementary Information, S3.3). The model reveals more complex behaviour for short nanowires, which prefer to align orthogonally to the beam axis. In this configuration they are exposed to polarization states that vary continuously along the beam axis, between circular polarization (producing rotation), to oblique linear polarization (associated with alignment). These scenarios are described in the Supporting Information, S3.3.

When more than one SiNW is held in the trap with PLP polarized beams, more complex stable arrangements are observed influenced by optical binding (see Section S7 in the Supp. Info.). SiNWs are trapped in close proximity and tend to orient parallel or perpendicularly to

each other (Fig. S17a). In this case, the arrangement of several particles is given partially by the influence of the standing wave. However, optical binding mediated by mutual scattering between SiNWs is also occurring.[76]

In crossed polarized, XLP, beams the distance, d, between SiNWs can be controlled with the beam waist, w_0, similarly as for spherical objects[19,75] (see Section S7 in the Supp. Info.). In larger beam waists the SiNWs are localized far apart while for narrow beam waists they tend to overlap in lateral direction and change their mutual orientation (Fig S17c). In particular, we find that d is comparable to the Rayleigh range z_{R} of the beams. When z_{R} becomes lower than the nanowire length, the particles arrange parallel to each other, creating a bundle that, probably due to the increased thickness and/or possible asymmetry in the shape, is expelled from the trap (see Movie 3).

The equilibrium configurations for single long nanowires are well reproduced by the theoretical model for both PLP and XLP beams (see Supporting Information S3.1, S3.3). Further simulations show some of the interaction effects referred to above. In particular, forces on nanowires appear to be strengthened by optical binding effects amongst pairs of nanowires, resulting in enhanced stiffness coefficients and increasingly stable structures. This is described in detail in the Supplementary Information S3.1.3 and S3.2.2.

Finally, we note that non-conservative cycling, as previously described,[28,29,96] will be present whenever an equilibrium configuration has sufficiently low symmetry to permit non-symmetric coupling between different degrees of freedom. For example, a SiNW trapped in a PLP configuration, aligned with the polarization and with its centre on the beam axis, will be at equilibrium, because there is no possibility for asymmetric coupling between degrees of freedom. However, if the symmetry is reduced, for example, if the SiNW has a taper,[29] or a bend,[39] or if its centre is displaced from the beam axis, then we expect to see non-conservative effects. Similarly, optically bound SiNW will show non-conservative cycling whenever they find themselves in an equilibrium configuration with sufficiently low symmetry.[31]

Circular polarization. We realize a circular polarized counter-propagating trap by simply

inserting a quarter waveplate in the path of each beam and set their fast axes to ± 45 degrees with respect to the incident beam polarization. When the two counter-propagating beams have opposite circular polarizations, σ^+/σ^- configuration, their superposition gives a standing wave in which the electric field rotates around the beam propagation axis.[21,31] As with the linearly polarized trap (PLP), the interference fringes support a variety of equilibrium orientations. We observe SiNWs stably oriented both perpendicularly or along the beam propagation direction. In the case of perpendicular orientation, spin angular momentum[31,93,97] is efficiently transferred from the circularly polarized light to the trapped SiNWs (see Fig. 3(a)). This causes them to rotate continuously with a rotational frequency dependent on SiNW length, the shorter the nanowire the higher the frequency of rotation. Moreover, we observe that for a transverse orientation the SiNWs can rotate efficiently when their fixed point corresponds to their centre or to one of their edges.

The rotational dynamics of the trapped particles is studied with both video microscopy[21] and correlation function analysis of the QPD tracking signals.[26,28,33,39,98] In particular, in the latter case, we characterize the rotational motion of SiNWs by analyzing the transverse (xy plane) differential cross-correlation functions,[28,98] $DCCF_{xy}(\tau) = CCF_{xy}(\tau) - CCF_{yx}(\tau)$, where $CCF_{xy} = \langle V_x(t)V_y(t+\tau)\rangle / \sqrt{\langle V_x^2(t)\rangle \langle V_y^2(t)\rangle}$ represents the normalized cross-correlation function between tracking signals along the x and y axes as a function of lag time, τ. Thus, rotations about the z axis appear in the $DCCF_{xy}$ as a sinusoidal oscillation with frequency related to the trapped particle rotational frequency.[28,98] In Fig. 3(b) we show a typical $DCCF_{xy}$ of a rotating nanowire with a length $L \approx 3$ μm, together with the corresponding tracking signal (V_x) shown in the inset. The $DCCF_{xy}$ data is fitted with a simple sinusoidal function:[28,98]

$$DCCF_{xy} = A \sin(2\Omega\tau) \tag{1}$$

where Ω is the rotational angular frequency of the nanowire with the factor 2 related to the SiNW symmetry,[39] and A is a constant related with a calibration factor. From the fit of the $DCCF_{xy}$ corresponding to three different tracks, we obtain an average rotational

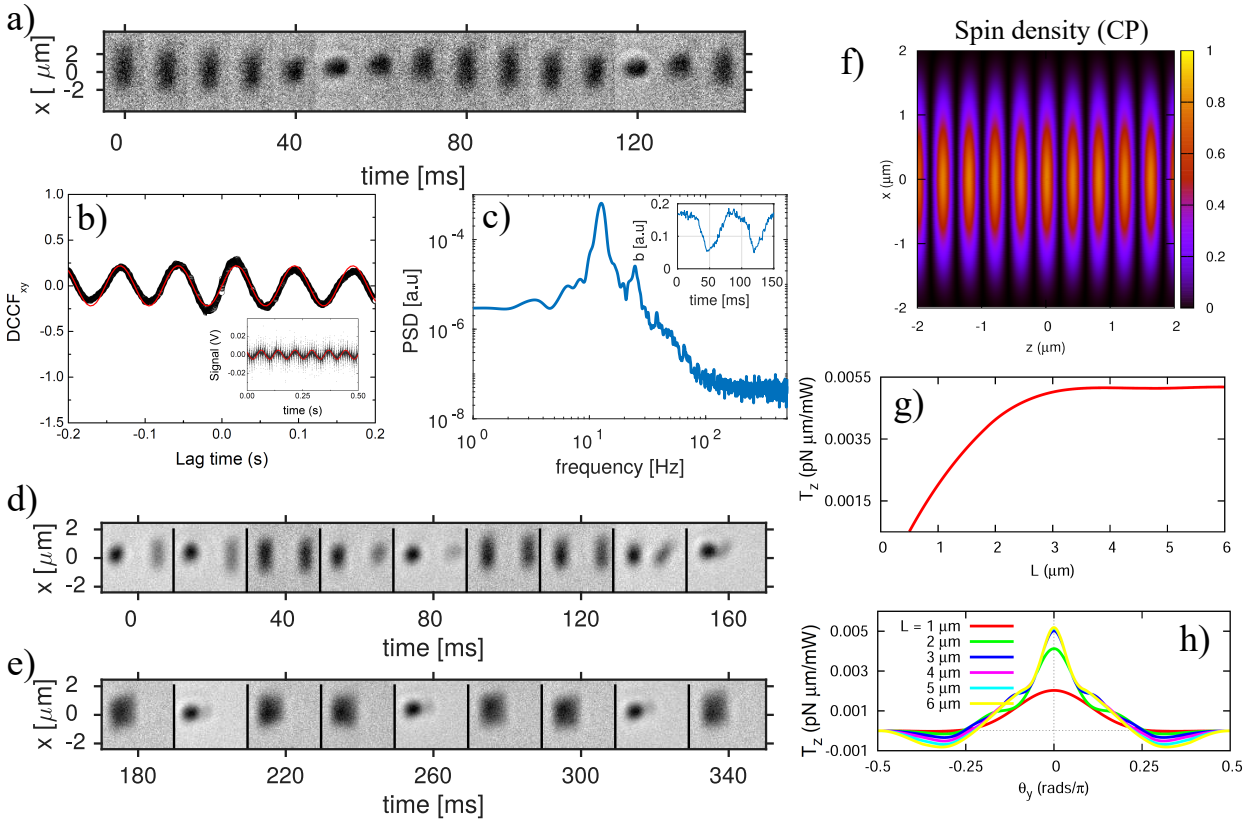

Figure 3: Optical trapping and rotations of SiNWs in σ^+/σ^- circular polarization of counter-propagating beams. (a) Image sequence, from Movie 4, of a nanowire with a length $L \approx 3$ μm rotating with respect to the beam propagation axis. (b) Transverse differential cross-correlation function, $DCCF_{xy}$, obtained from the transverse QPD tracking signals (inset). The fit (red line) with a sinusoidal function (Eq. 1) to the data gives account of the rotational dynamics of the trapped SiNW. (c) Power spectrum analysis of the aspect ratio modulation (inset) of the SiNW image obtained from video microscopy (see Supporting Information). The frequency of the peak in the power spectrum is two times the rotational frequency of the SiNW, and it is consistent with the rotational frequency obtained from DCCF analysis of the QPD tracking. (d-e) Image sequences from Movie 5. Two SiNWs initially displaced far from each other rotate independently. When they approach next to each other, their rotation synchronizes and locks parallel orientation due to hydrodynamic interactions. (f) Calculated spin density, $\sigma = 2\Re(E_x E_y^*)$ (g) Calculated rotational torque, T_z, as a function of SiNW length. (h) Optical torque, T_z on obliquely oriented nanowires, where θ_y is the angle that the axis of the nanowire makes with the x axis. Note how these obliquely oriented wires also experience a rotational torque about the beam axis which even reverses its sign for $\theta_y > 0.25\pi$.

angular frequency $\Omega = 42 \pm 1$ rad/s, from which a rotational frequency is obtained as $f_{\rm rot} = \Omega/2\pi = 6.7 \pm 0.2$ Hz. This is consistent with the rotational frequency, $f_{\rm rot} \approx 6.4$ Hz, that we obtain independently following a power spectral density (PSD) analysis, shown in Fig. 3c, of the SiNW rotational dynamics obtained from video microscopy (see Supporting Information). The rotational dynamics of the SiNW is a balance between the spinning optical torque, T_z, and the viscous rotational drag torque related to the SiNW rotational mobility (see Supporting Information), $\Gamma_{\rm rot} \approx 104$ $(\mathrm{pN}\,\mu\mathrm{m\,s})^{-1}$. Thus, by measuring the rotational angular frequency we also get an estimate of the optical spinning torque, $T_z = \Omega/\Gamma_{\rm rot} \approx 0.4$ pN μm. It is worth noting that the observed rotational dynamics for our SiNWs is slower than that observed for plasmonic nanoparticles.[99,100] This is because our SiNWs are not absorbing light and the transfer of spin angular momentum occurs because of the anisotropic scattering related to the non-spherical shape.[97] Furthermore, the analysis of the autocorrelation functions (ACFs) has also proved useful to get information on the center-of-mass fluctuations of non-spherical nanostructures in standard optical traps.[11,26,33] In fact, the exponential decay rates of ACFs, ω_x, ω_y, ω_z, are related to translational fluctuations that provide optical force stiffnesses through the knowledge of the anisotropic hydrodynamic mobilities of the SiNWs (see Supporting Information). Thus, for the axial direction $k_z = \omega_z/\Gamma_\perp$ is the trap stiffness corresponding to the tighter confinement, where $\Gamma_\perp$ (≈ 114 $\mu\mathrm{m\,pN^{-1}\,s^{-1}}$ for our SiNW) is the transverse translational mobility.[33] From the data we obtain an axial relaxation rate of $\omega_z = 331 \pm 83$ rad/s, from which the axial spring constant $k_z \approx 2.9\,\mathrm{pN}/\mu\mathrm{m}$ is obtained. Instead, to estimate the radial force constant we can introduce the radial relaxation frequency $\omega_\rho = (\omega_x + \omega_y)/2$, by averaging the relaxation rate of the corresponding transverse ACFs, C_{xx} and C_{yy}, and the radial mobility, $\Gamma_\rho = (\Gamma_\parallel + \Gamma_\perp)/2$ (≈ 142 $\mu\mathrm{m\,pN^{-1}\,s^{-1}}$ for our SiNW), by averaging the transverse and parallel mobilities (see Supporting Information). These values allow the calculation of the radial spring constants $k_\rho \approx 0.8\,\mathrm{pN}/\mu\mathrm{m}$, that is about 3.6 times smaller than the axial one, k_z, consistently with the standing wave intensity pattern.

Optical binding is also observed in σ^+/σ^- configuration. In Fig. 3 (d-e), an image sequence is shown (Movie 5). Two spinning SiNWs rotate independently from each other if they are placed far from each other. As they get closer, they achieve rotational synchronization and orient parallel to each other during the synchronized rotation. A behaviour similar to what is expected for pairs of SiNWs in counter-propagating σ^+/σ^- plane waves.[31] SiNWs alignment during rotational motion is due to both the optical binding between them and to their hydrodynamic synchronization that appear to occur at a short range. In contrast, for larger polystyrene micro-discs synchronization has been observed for larger distances and perpendicular orientation was kept even for discs in contact.[21,84] This shows that size and shape of the trapped particles play a key role in their binding and hydrodynamic interactions controlling the range and strength of synchronization and binding.

We also observed rotation of more than two SiNWs (see Movie 6). However in agreement with theoretical results,[31] rotation of many SiNWs is not synchronized even for large rotational frequencies and for close proximity of the trapped particles. As a proof of the complexity of these geometries, we also observed mixed configurations of periodically displaced SiNWs aligned parallel and rotating SiNWs oriented perpendicular to the beam propagation axis (see Movie 7). Finally, we verified that the rotation stops when the beam polarization is switched from circular to linear (horizontal or vertical).

Most of the effects described above are faithfully reproduced by our models (Supporting Information, S3.2), including the rotation and equilibrium orientations of single nanowires, and the coupled rotations of pairs of SiNWs. The simulations show that rotational optical binding effects serve to hold pairs of rotating wires in an approximately parallel configuration. The pair of wires then rotate in synchrony, remaining parallel despite the diffusive influence of thermal fluctuations. The strength of this optical interaction decreases with increasing separation but is, nonetheless, of relatively long range. For instance, the rotational interaction between 6 μm long nanowires, remains significant for separations of 10 μm, enabling synchronous motion at modest beam powers of $\sim$ 10 mW.

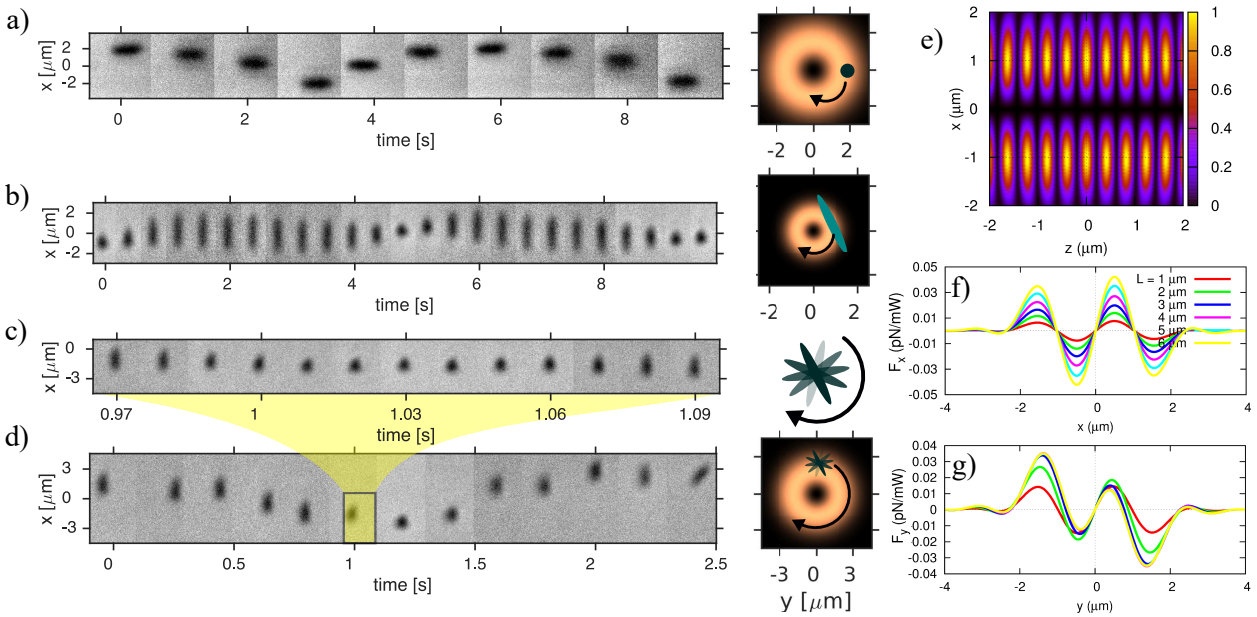

Figure 4: Optical trapping and rotations of SiNWs in counter-propagating circularly polarized Laguerre-Gaussian beams. The topological charge is $l = \pm 1$. In (a), the nanowire is aligned parallel to the beam propagation axis. A clear orbital motion around the optical vortex is observed (Movie 8). In (b), the nanowire is aligned perpendicularly to the beam propagation axis and we observe orbiting combined with a reorientation of the SiNW (Movie 9) resulting from the transfer of both spin and orbital angular momentum of light. In (c) and (d), the simultaneous spinning and orbiting of a shorter nanowire is observed (Movie 10). On the right part of the figure, the cross sections of the beam are shown with sketches of the trapped nanowire. (e) Intensity field for the Laguerre-Gaussian beam in the yz plane (f) Calculated restoring forces on a nanowire aligned with the beam axis and displaced in the x direction. The plot shows a possible off-axis equilibrium position with the wire aligned within the beam axis. (g) Restoring forces on a wire aligned with the x axis and displaced along the y axis, showing another off-axis equilibrium orientation with the wire aligned normally to the beam axis. In both (e) and (g) these off-axis equilibria positions are related to the doughnut shaped intensity profile in the xy plane of the Laguerre-Gaussian beams.

Laguerre-Gaussian beams with linear and circular polarization. We extended our investigation to include the transfer of orbital angular momentum (OAM) on the trapped SiNWs from two counter-propagating Laguerre-Gaussian beams with topological charge was $l = \pm 1$. The polarization state of the two beams are controlled independently as in the previous experiments so that we can switch from linear to circular polarization by means of quarter waveplates placed on the counter-propagating beams path. When we set circular polarization with opposite helicity, we observe again different stable orientations that depend on the SiNW length. Figure 4a and Movie 8 show a SiNW bundle thicker than an individual one stably oriented parallel to the beam propagation axis. A clear orbital motion off-centered with respect to the beam axis resulting from the transfer of OAM from the beams to the wire is observed both in linear and circular polarizations. However, when the SiNW gets shorter the orientation is flipped and the SiNW lies in the transverse plane, *i.e.*, perpendicularly to the beam propagation. In this case, circular polarization of the beams results in an intrinsic rotation about the SiNW symmetry axis superposed to an off-centered orbital motion of the SiNW centre-of-mass. This combined influence of spin and OAM[101] of light upon an object is shown in Fig. 4b and Movie 9. In this case, spin and orbital rotations of the trapped SiNW have about the same frequency of ~ 0.1 Hz. This effect is more clearly demonstrated in Fig. 4c and Movie 10 for a SiNW much shorter than the beam typical transverse size. Here the spinning rotational frequency is about 4.5 Hz and the intrinsic spinning, of about 0.5 Hz, is better separated from the orbiting rotational motion resulting in a clear separation in the image sequence extracted from the movie acquired with the camera.

Once again, this rich controlled phenomenology is well replicated by our models (Supporting Information S3.4). As with the experiment, SiNWs can orient themselves parallel or perpendicular to the beam axis. Gradient forces cause the centre of mass of the SiNW to trap off axis, while orbital angular momentum causes the wire to precess about the beam axis. In addition, short SiNWs can strongly interact both with the spin angular momentum, which causes them to rotate about their own centres, and the orbital momentum of

the beam, which their centres to rotate about the beam axis. Movies of the simulations are provided as Supporting Information.

In conclusion, we described a systematic investigation of behaviors of single or multiple SiNWs trapped in counter-propagating Gaussian or Laguerre-Gaussian beams with different polarization properties. We demonstrated that single SiNWs with length in the range of several microns, *i.e.*, longer than the typical beam transverse size, prefer a stable orientation along the propagation axis for all polarization states. On the other hand, shorter SiNWs arrange preferentially along the transverse polarization axis. This interplay between the torque exerted by the high intensity gradients and the polarization torque is controlled by the particle length. When multiple SiNWs self-arrange along the beam axis, their mutual distance can be tuned with the width of the beams' waists. In circularly polarized beams, spin angular momentum is transferred to the trapped SiNWs oriented perpendicularly to the beam propagation resulting in light-driven nano-rotors. Finally, SiNWs confined in counter-propagating Laguerre-Gaussian beams with opposite topological charge tend to orbit around the beam axis and for circularly polarized beams they also spin about their symmetry axis demonstrating how shape can couple spin and orbital angular momentum of light. The negligible absorption in the infrared by our native SiNWs can represent an intriguing aspect for their optical manipulation in biological environments, where large heating effects might be detrimental. On the other hand, recent experiments have also shown great potential for photodynamic therapy applications,[86] as optically trapped SiNWs can photosensitize singlet-oxygen, as well as photothermal therapy[91] when ion-implanted to increase photothermal heating. As far as optical trapping and binding is concerned, the difference between spheres and nanowires is associated with orientation, especially regarding polarization effects and rotational coupling between multiple objects. On the other hand, there is no fundamental difference between nanowires and spheroids (nanowires are very high aspect ratio spheroids). What differences there are depend, therefore, on the magnitude of the aspect ratio. The most significant qualitative difference is seen in rotational synchronization: micron sized spheroids

synchronize with their symmetry axes at right angles, nanowires synchronize with their axes parallel. This rich scenario has been elucidated also by means of accurate theoretical calculations of the optical and hydrodynamic interactions. We find that the extended shape of the nanowires increases the variety of configurations and dynamical processes that can be optically excited and controlled over the large capture range of counter-propagating optical traps.

Supporting Information. Forces and torques on high aspect nanowires, numerical model, counter propagating beams, silicon nanowire preparation and characterization, silicon nanowire hydrodynamic coefficients, video microscopy, optical binding of nanowires in linearly polarized beams, movie captions, additional references.

Acknowledgement

The authors acknowledge support by The Joint Bilateral Project CNR-16-12 between the Italian National Research Council (CNR) and the Czech Academy of Science, Czech Science Foundation (GB14-36681G) and Ministry of Education, Youth and Sports of the Czech Republic (LO1212) and European Commission (CZ.1.05/2.1.00/01.0017).

References

(1) Samorì, P., Ed. *Scanning probe microscopies beyond imaging: manipulation of molecules and nanostructures*; John Wiley & Sons, 2006.

(2) Ashkin, A. Acceleration and trapping of particles by radiation pressure. *Phys. Rev. Lett.* **1970**, *24*, 156–159.

(3) Ashkin, A.; Dziedzic, J.; Bjorkholm, J.; Chu, S. Observation of a single-beam gradient optical trap for dielectric particles. *Opt. Lett.* **1986**, *11*, 288–290.

(4) Jones, P. H.; Maragò, O. M.; Volpe, G. *Optical tweezers: Principles and applications*; Cambridge University Press: Cambridge, 2015.

(5) Jonáš, A.; Zemánek, P. Light at work: The use of optical forces for particle manipulation, sorting, and analysis. *Electophoresis* **2008**, *29*, 4813–4851.

(6) Maragò, O. M.; Jones, P. H.; Gucciardi, P. G.; Volpe, G.; Ferrari, A. C. Optical trapping and manipulation of nanostructures. *Nature Nanotechnol.* **2013**, *8*, 807–819.

(7) Spesyvtseva, S. E. S.; Dholakia, K. Trapping in a material world. *ACS Photon.* **2016**, *3*, 719–736.

(8) Polimeno, P.; Magazzù, A.; Iatì, M. A.; Patti, F.; Saija, R.; Degli Esposti Boschi, C.; Donato, M. G.; Gucciardi, P. G.; Jones, P. H.; Volpe, G.; Maragò, O. M. Optical tweezers and their applications. *Journal of Quantitative Spectroscopy & Radiative Transfer* **2018**, *218*, 131–150.

(9) Nedev, S.; Urban, A. S.; Lutich, A. A.; Feldmann, J. Optical force stamping lithography. *Nano Lett.* **2011**, *11*, 5066–5070.

(10) Gargiulo, J.; Violi, I. L.; Cerrota, S.; Chvátal, L.; Cortès, E.; Perassi, E. M.; Diaz, F.; Zemánek, P.; Stefani, F. D. Accuracy and Mechanistic Details of Optical Printing of Single Au and Ag Nanoparticles. *ACS nano* **2017**, *11*, 9678–9688.

(11) Donato, M. G.; Messina, E.; Foti, A.; Smart, T. J.; Jones, P. H.; Iatì, M. A.; Saija, R.; Gucciardi, P. G.; Maragò, O. M. Optical trapping and optical force positioning of two-dimensional materials. *Nanoscale* **2018**, *10*, 1245–1255.

(12) Burns, M. M.; Fournier, J.-M.; Golovchenko, J. A. Optical binding. *Physical Review Letters* **1989**, *63*, 1233–1236.

(13) Dholakia, K.; Zemánek, P. Gripped by light: Optical binding. *Rev. Mod. Phys.* **2010**, *82*, 1767–1791.

(14) Bowman, R. W.; Padgett, M. J. Optical trapping and binding. *Reports on Progress in Physics* **2013**, *76*, 026401.

(15) Brzobohatý, O.; Čižmár, T.; Karásek, V.; Šiler, M.; Dholakia, K.; Zemánek, P. Experimental and theoretical determination of optical binding forces. *Opt. Express* **2010**, *18*, 25389–25402.

(16) Nakayama, Y.; Pauzauskie, P. J.; Radenovic, A.; Onorato, R. M.; Saykally, R. J.; Liphardt, J.; Yang, P. Tunable nanowire nonlinear optical probe. *Nature* **2007**, *447*, 1098–1102.

(17) Neves, A. A. R.; Camposeo, A.; Pagliara, S.; Saija, R.; Borghese, F.; Denti, P.; Iatì, M. A.; Cingolani, R.; Maragò, O. M.; Pisignano, D. Rotational dynamics of optically trapped nanofibers. *Opt. Express* **2010**, *18*, 822–830.

(18) Tatarkova, S. A.; Carruthers, A. E.; Dholakia, K. One-Dimensional Optically Bound Arrays of Microscopic Particles. *Phys. Rev. Lett.* **2002**, *89*, 283901.

(19) Karásek, V.; Čižmár, T.; Brzobohatý, O.; Zemánek, P.; Garcés-Chávez, V.; Dholakia, K. Long-range one-dimensional longitudinal optical binding. *Phys. Rev. Lett.* **2008**, *101*, 143601.

(20) Skelton, S. E.; Sergides, M.; Patel, R.; Karczewska, E.; Maragò, O. M.; Jones, P. H. Evanescent wave optical trapping and transport of micro-and nanoparticles on tapered optical fibers. *Journal of Quantitative Spectroscopy and Radiative Transfer* **2012**, *113*, 2512–2520.

(21) Brzobohatý, O.; Arzola, A. V.; Šiler, M.; Chvátal, L.; Jákl, P.; Simpson, S.; Zemánek, P. Complex rotational dynamics of multiple spheroidal particles in a circularly polarized, dual beam trap. *Opt. Express* **2015**, *23*, 7273–7287.

(22) Han, X.; Jones, P. H. Evanescent wave optical binding forces on spherical microparticles. *Optics letters* **2015**, *40*, 4042–4045.

(23) Han, X.; Luo, H.; Xiao, G.; Jones, P. H. Optically bound colloidal lattices in evanescent optical fields. *Optics letters* **2016**, *41*, 4935–4938.

(24) Agarwal, R.; Ladavac, K.; Roichman, Y.; Yu, G.; Lieber, C. M.; Grier, D. G. Manipulation and assembly of nanowires with holographic optical traps. *Optics Express* **2005**, *13*, 8906–8912.

(25) Pauzauskie, P. J.; Radenovic, A.; Trepagnier, E.; Shroff, H.; Yang, P.; Liphardt, J. Optical trapping and integration of semiconductor nanowire assemblies in water. *Nature Materials* **2006**, *5*, 97–101.

(26) Irrera, A.; Artoni, P.; Saija, R.; Gucciardi, P. G.; Iatì, M. A.; Borghese, F.; Denti, P.; Iacona, F.; Priolo, F.; Maragò, O. M. Size-Scaling in Optical Trapping of Silicon Nanowires. *Nano Lett.* **2011**, *11*, 4879–4884.

(27) Reece, P. J.; Toe, W. J.; Wang, F.; Paiman, S.; Gao, Q.; Tan, H. H.; Jagadish, C. Characterization of semiconductor nanowires using optical tweezers. *Nano Lett.* **2011**, *11*, 2375–2381.

(28) Irrera, A.; Magazzù, A.; Artoni, P.; Simpson, S. H.; Hanna, S.; Jones, P. H.; Priolo, F.; Gucciardi, P. G.; Maragò, O. M. Photonic torque microscopy of the nonconservative force field for optically trapped silicon nanowires. *Nano letters* **2016**, *16*, 4181–4188.

(29) Toe, W. J.; Ortega-Piwonka, I.; Angstmann, C. N.; Gao, Q.; Tan, H. H.; Jagadish, C.; Henry, B. I.; Reece, P. J. Nonconservative dynamics of optically trapped high-aspect-ratio nanowires. *Physical Review E* **2016**, *93*, 022137.

(30) Kuhn, S.; Kosloff, A.; Stickler, B. A.; Patolsky, F.; Hornberger, K.; Arndt, M.;

Millen, J. Full rotational control of levitated silicon nanorods. *Optica* **2017**, *4*, 356–360.

(31) Simpson, S. H.; Zemánek, P.; Maragò, O. M.; Jones, P. H.; Hanna, S. Optical Binding of Nanowires. *Nano Letters* **2017**, *17*, 3485–3492.

(32) Maragò, O. M.; Gucciardi, P. G.; Bonaccorso, F.; Calogero, G.; Scardaci, V.; Rozhin, A. G.; Ferrari, A. C.; Jones, P. H.; Saija, R.; Borghese, F.; Iatì, M. A. Optical trapping of carbon nanotubes. *Physica E: Low-dimensional Systems and Nanostructures* **2008**, *40*, 2347–2351.

(33) Maragò, O. M.; Jones, P. H.; Bonaccorso, F.; Scardaci, V.; Gucciardi, P. G.; Rozhin, A. G.; Ferrari, A. C. Femtonewton Force Sensing with Optically Trapped Nanotubes. *Nano Lett.* **2008**, *8*, 3211–3216.

(34) Maragò, O. M.; Bonaccorso, F.; Saija, R.; Privitera, G.; Gucciardi, P. G.; Iatì, M. A.; Calogero, G.; Jones, P. H.; Borghese, F.; Denti, P.; Nicolosi, V.; Ferrari, A. C. Brownian motion of graphene. *ACS Nano* **2010**, *4*, 7515–7523.

(35) Donato, M. G.; Vasi, S.; Sayed, R.; Jones, P. H.; Bonaccorso, F.; Ferrari, A. C.; Gucciardi, P. G.; Maragò, O. M. Optical trapping of nanotubes with cylindrical vector beams. *Opt. Lett.* **2012**, *37*, 3381–3383.

(36) Svoboda, K.; Block, S. M. Optical trapping of metallic Rayleigh particles. *Opt. Lett.* **1994**, *19*, 930–932.

(37) Lehmuskero, A.; Johansson, P.; Rubinsztein-Dunlop, H.; Tong, L.; Kall, M. Laser trapping of colloidal metal nanoparticles. *ACS Nano* **2015**, *9*, 3453–3469.

(38) Selhuber-Unkel, C.; Zins, I.; Schubert, O.; Sönnichsen, C.; Oddershede, L. B. Quantitative optical trapping of single gold nanorods. *Nano Lett.* **2008**, *8*, 2998–3003.

(39) Jones, P. H.; ; Palmisano, F.; Bonaccorso, F.; Gucciardi, P. G.; Calogero, G.; Ferrari, A. C.; Maragò, O. M. Rotation detection in light-driven nanorotors. *ACS Nano* **2009**, *3*, 3077–3084.

(40) Yan, Z.; Jureller, J. E.; Sweet, J.; Guffey, M. J.; Pelton, M.; Scherer, N. F. Three-dimensional optical trapping and manipulation of single silver nanowires. *Nano Lett.* **2012**, *12*, 5155–5161.

(41) Messina, E.; Donato, M. G.; Zimbone, M.; Saija, R.; Iatì, M. A.; Calcagno, L.; Fragala, M. E.; Compagnini, G.; D'Andrea, C.; Foti, A.; Gucciardi, P. G.; Maragò, O. M. Optical trapping of silver nanoplatelets. *Opt. Express* **2015**, *23*, 8720–8730.

(42) Brzobohatý, O.; Šiler, M.; Trojek, J.; Chvátal, L.; Karásek, V.; Paták, A.; Pokorná, Z.; Mika, F.; Zemánek, P. Three-Dimensional Optical Trapping of a Plasmonic Nanoparticle using Low Numerical Aperture Optical Tweezers. *Scientific Reports* **2015**, *5*, 8106.

(43) Spadaro, D.; Iatì, M. A.; Donato, M. G.; Gucciardi, P. G.; Saija, R.; Cherlakola, A. R.; Scaramuzza, S.; Amendola, V.; Maragò, O. M. Scaling of optical forces on Au–PEG core–shell nanoparticles. *RSC Adv.* **2015**, *5*, 93139–93146.

(44) Spadaro, D.; Iatì, M. A.; Pérez-Piñeiro, J.; Vázquez-Vázquez, C.; Correa-Duarte, M. A.; Donato, M. G.; Gucciardi, P. G.; Saija, R.; Strangi, G.; Maragò, O. M. Optical Trapping of Plasmonic Mesocapsules: Enhanced Optical Forces and SERS. *The Journal of Physical Chemistry C* **2016**, *121*, 691–700.

(45) Ashkin, A.; Dziedzic, J. M. Optical trapping and manipulation of viruses and bacteria. *Science* **1987**, *235*, 1517–1520.

(46) Ashkin, A.; Dziedzic, J. Internal cell manipulation using infrared laser traps. *Proceedings of the National Academy of Sciences* **1989**, *86*, 7914–7918.

(47) Fazal, F. M.; Block, S. M. Optical tweezers study life under tension. *Nature Photonics* **2011**, *5*, 318–321.

(48) van der Horst, A.; van Oostrum, P. D.; Moroz, A.; van Blaaderen, A.; Dogterom, M. High trapping forces for high-refractive index particles trapped in dynamic arrays of counterpropagating optical tweezers. *Applied optics* **2008**, *47*, 3196–3202.

(49) Yan, Z.; Pelton, M.; Vigderman, L.; Zubarev, E.; Scherer, N. Why Single-Beam Optical Tweezers Trap Gold Nanowires in Three Dimensions. *ACS Nano* **2013**, *7*, 8794–8800.

(50) Zemánek, P.; Jonáš, A.; Liška, M. Simplified description of optical forces acting on a nanoparticle in the Gaussian standing wave. *J. Opt. Soc. Am. A* **2002**, *19*, 1025–1034.

(51) Čižmár, T.; Šiler, M.; Zemánek, P. An optical nanotrap array movable over a milimetre range. *Appl. Phys. B* **2006**, *84*, 197–203.

(52) Zemánek, P.; Jonáš, A.; Šrámek, L.; Liška, M. Optical trapping of nanoparticles and microparticles using Gaussian standing wave. *Opt. Lett.* **1999**, *24*, 1448–1450.

(53) Pitzek, M.; Steiger, R.; Thalhammer, G.; Bernet, S.; Ritsch-Marte, M. Optical mirror trap with a large field of view. *Optics express* **2009**, *17*, 19414–19423.

(54) Constable, A.; Kim, J. Demonstration of a fiber-optical light-force trap. *Opt. Lett.* **1993**, *18*, 1867–1869.

(55) Guck, J.; Ananthakrishnan, R.; Mahmood, H.; Moon, T. J.; Cunningham, C. C.; Käs, J. The optical stretcher: a novel laser tool to micromanipulate cells. *Biophysical journal* **2001**, *81*, 767–784.

(56) Gherardi, D. M.; Carruthers, A. E.; Čižmár, T.; Wright, E. M.; Dholakia, K. A dual beam photonic crystal fibre trap for microscopic particles. *Appl. Phys. Lett.* **2008**, *93*, 041110.

(57) Schmidt, O. A.; Euser, T. G.; Russell, P. S. Mode-based microparticle conveyor belt in air-filled hollow-core photonic crystal fiber. *Opt. Express* **2013**, *21*, 29383–29391.

(58) Grass, D.; Fesel, J.; Hofer, S. G.; Kiesel, N.; Aspelmeyer, M. Optical trapping and control of nanoparticles inside evacuated hollow core photonic crystal fibers. *Appl. Phys. Lett.* **2016**, *108*, 221103.

(59) Singer, W.; Frick, M.; Bernet, S.; Ritsch-Marte, M. Self-organized array of regularly spaced microbeads in a fiber-optical trap. *JOSA B* **2003**, *20*, 1568–1574.

(60) Ng, J.; Lin, Z. F.; Chan, C. T.; Sheng, P. Photonic clusters formed by dielectric microspheres: Numerical simulations. *Phys. Rev. B* **2005**, *72*, 085130.

(61) Bradshaw, D. S.; Andrews, D. L. Optically induced forces and torques: Interactions between nanoparticles in a laser beam. *Phys. Rev. A* **2005**, *72*, 033816.

(62) Grzegorczyk, T. M.; Kemp, B. A.; Kong, J. A. Trapping and binding of an arbitrary number of cylindrical particles in an in-plane electromagnetic field. *J. Opt. Soc. Am. A* **2006**, *23*, 2324–2330.

(63) Metzger, N. K.; Wright, E. M.; Dholakia, K. Theory and simulation of the bistable behaviour of optically bound particles in the Mie size regime. *New. J. Phys.* **2006**, *8*, 139.

(64) Karásek, V.; Dholakia, K.; Zemánek, P. Analysis of optical binding in one dimension. *Appl. Phys. B* **2006**, *84*, 149–156.

(65) Karásek, V.; Zemánek, P. Analytical description of longitudinal optical binding of two spherical nanoparticles. *J. Opt. A: Pure Appl. Opt.* **2007**, *9*, S215–S220.

(66) Taylor, J. M.; Wong, L. Y.; Bain, C. D.; Love, G. D. Emergent properties in optically bound matter. *Opt. Express* **2008**, *16*, 6921–6928.

(67) Chvátal, L.; Brzobohatý, O.; Zemánek, P. Binding of a pair of Au nanoparticles in a wide Gaussian standing wave. *Opt. Rev.* **2015**, *22*, 157–161.

(68) Karásek, V.; Šiler, M.; Brzobohatý, O.; Zemánek, P. Dynamics of an optically bound structure made of particles of unequal sizes. *Opt. Lett.* **2017**, *42*, 1436–1439.

(69) Burns, M. M.; Fournier, J.-M.; Golovchenko, J. A. Optical Matter: Crystallization and Binding in Intense Optical Fields. *Science* **1990**, *249*, 749–754.

(70) Guillon, M.; Moine, O.; Stout, B. Longitudinal optical binding of high optical contrast microdroplets in air. *Phys. Rev. Lett.* **2006**, *96*, 143902.

(71) Metzger, N. K.; Dholakia, K.; Wright, E. M. Observation of Bistability and Hysteresis in Optical Binding of Two Dielectric Spheres. *Phys. Rev. Lett.* **2006**, *96*, 068102.

(72) Metzger, N. K.; Marchington, R. F.; Mazilu, M.; Smith, R. L.; Dholakia, K.; Wright, E. M. Measurement of the Restoring Forces Acting on Two Optically Bound Particles from Normal Mode Correlations. *Phys. Rev. Lett.* **2007**, *98*, 068102.

(73) Taylor, J.; Love, G. Optical binding mechanisms: a conceptual model for Gaussian beam traps. *Optics Express* **2009**, *17*, 15381–15389.

(74) Čižmár, T.; Brzobohatý, O.; Dholakia, K.; Zemánek, P. The holographic optical micromanipulation system based on counter-propagating beams. *Laser Phys. Lett.* **2011**, *8*, 50–56.

(75) Brzobohatý, O.; Karásek, V.; Čižmár, T.; Zemánek, P. Dynamic size tuning of multidimensional optically bound matter. *Appl. Phys. Lett.* **2011**, *99*, 101105.

(76) Brzobohatý, O.; Karásek, V.; Šiler, M.; Trojek, J.; Zemánek, P. Static and dynamic behavior of two optically bound microparticles in a standing wave. *Opt. Express* **2011**, *19*, 19613–19626.

(77) Demergis, V.; Florin, E.-L. Ultrastrong Optical Binding of Metallic Nanoparticles. *Nano Lett.* **2012**, *12*, 5756–5760.

(78) Yan, Z.; Gray, S. K.; Scherer, N. F. Potential energy surfaces and reaction pathways for light-mediated self-organization of metal nanoparticle clusters. *Nature Communications* **2014**, *5*, 3751.

(79) Brzobohatý, O.; Karásek, V.; Šiler, M.; Chvátal, L.; Čizmár, T.; Zemánek, P. Experimental demonstration of optical transport, sorting and self-arrangement using a 'tractor beam'. *Nature Photon.* **2013**, *7*, 123–127.

(80) Damková, J.; Chvátal, L.; Ježek, J.; Oulehla, J.; Brzobohatý, O.; Zemánek, P. Enhancement of the 'tractor-beam' pulling force on an optically bound structure. *Light-Sci. Appl.* **2018**, *7*, 17135.

(81) Arita, Y.; Mazilu, M.; Vettenburg, T.; Wright, E. M.; Dholakia, K. Rotation of two trapped microparticles in vacuum: observation of optically mediated parametric resonances. *Opt. Lett.* **2015**, *40*, 4751–4754.

(82) Brzobohatý, O.; Hernandez, R. J.; Simpson, S.; Mazzulla, A.; Cipparrone, G.; Zemánek, P. Chiral particles in the dual-beam optical trap. *Opt. Express* **2016**, *24*, 26382–26391.

(83) Andrews, D. L.; Bradshaw, D. S. Laser-induced forces between carbon nanotubes. *Opt. Lett.* **2005**, *30*, 783–785.

(84) Simpson, S. H.; Chvatal, L.; Zemanek, P. Synchronization of colloidal rotors through angular optical binding. *Phys. Rev. A* **2016**, *93*, 023842.

(85) Casiello, M.; Picca, R. A.; Fusco, C.; D'Accolti, L.; Leonardi, A. A.; Lo Faro, M. J.; Irrera, A.; Trusso, S.; Cotugno, P.; Sportelli, M. C.; Cioffi, N.; Nacci, A. Catalytic

activity of silicon nanowires decorated with gold and copper nanoparticles deposited by pulsed laser ablation. *Nanomaterials* **2018**, *8*, 78.

(86) Smith, B. E.; Roder, P. B.; Hanson, J. L.; Manandhar, S.; Devaraj, A.; Perea, D. E.; Kim, W.-J.; Kilcoyne, A. D.; Pauzauskie, P. J. Singlet-Oxygen Generation from Individual Semiconducting and Metallic Nanostructures during Near-Infrared Laser Trapping. *ACS Photonics* **2015**, *2*, 559–564.

(87) Martínez, L.; Segarra, M.; Fernandez, M.; Espiell, F. Kinetics of the dissolution of pure silver and silver-gold alloys in nitric acid solution. *Metallurgical Transactions B* **1993**, *24*, 827–837.

(88) Han, H.; Huang, Z.; Lee, W. Metal-assisted chemical etching of silicon and nanotechnology applications. *Nano today* **2014**, *9*, 271–304.

(89) Pesce, G.; Volpe, G.; Maragò, O. M.; Jones, P. H.; Gigan, S.; Sasso, A.; Volpe, G. Step-by-step guide to the realization of advanced optical tweezers. *J. Opt. Soc. Am. B-Opt. Phys.* **2015**, *32*, B84–B98.

(90) Roder, P. B.; Pauzauskie, P. J.; Davis, E. J. Nanowire Heating by Optical Electromagnetic Irradiation. *Langmuir* **2012**, *28*, 16177–16185.

(91) Roder, P. B.; Smith, B. E.; Davis, E. J.; Pauzauskie, P. J. Photothermal heating of nanowires. *The Journal of Physical Chemistry C* **2014**, *118*, 1407–1416.

(92) Simpson, S. H. Inhomogeneous and anisotropic particles in optical traps: Physical behaviour and applications. *Journal of Quantitative Spectroscopy and Radiative Transfer* **2014**, *146*, 81–99.

(93) Simpson, S. H.; Benito, D. C.; Hanna, S. Polarization-induced torque in optical traps. *Phys. Rev. A* **2007**, *76*, 043408.

(94) Borghese, F.; Denti, P.; Saija, R.; Iatì, M. A.; Maragò, O. M. Radiation Torque and Force on Optically Trapped Linear Nanostructures. *Phys. Rev. Lett.* **2008**, *100*, 163903.

(95) Simpson, S.; Hanna, S. Stability analysis and thermal motion of optically trapped nanowires. *Nanotechnology* **2012**, *23*, 205502.

(96) Simpson, S. H.; Hanna, S. First-order nonconservative motion of optically trapped nonspherical particles. *Phys. Rev. E* **2010**, *82*, 031141.

(97) Borghese, F.; Denti, P.; Saija, R.; Iatì, M. A. Radiation torque on nonspherical particles in the transition matrix formalism. *Optics Express* **2006**, *14*, 9508–9521.

(98) Volpe, G.; Petrov, D. Torque detection using Brownian fluctuations. *Phys. Rev. Lett.* **2006**, *97*, 210603.

(99) Lehmuskero, A.; Ogier, R.; Gschneidtner, T.; Johansson, P.; Käll, M. Ultrafast Spinning of Gold Nanoparticles in Water Using Circularly Polarized Light. *Nano Lett.* **2013**, *13*, 3129–3134.

(100) Shao, L.; Yang, Z.-J.; Andren, D.; Johansson, P.; Käll, M. Gold nanorod rotary motors driven by resonant light scattering. *ACS nano* **2015**, *9*, 12542–12551.

(101) Garcés-Chávez, V.; McGloin, D.; Padgett, M. J.; Dultz, W.; Schmitzer, H.; Dholakia, K. Observation of the Transfer of the Local Angular Momentum Density of a Multiringed Light Beam to an Optically Trapped Particle. *Phys. Rev. Lett.* **2003**, *91*, 093602.